RSC Advances

PAPER

View Article Online
View Journal | View Issue

Cite this: *RSC Adv.*, 2021, **11**, 18708

Inhibition effect of ZrF_4 on UO_2 precipitation in the LiF–BeF_2 molten salt

Hao Peng,[a] Yulong Song,[ab] Nan Ji,[a] Leidong Xie,[a] Wei Huang *[a] and Yu Gong [a]

The dissolution–precipitation behavior of zirconium dioxide (ZrO_2) in molten lithium fluoride–beryllium fluoride (LiF–BeF_2, (2 : 1 mol, FLiBe)) eutectic salt at 873 K was studied. The results of the dissolution experiment showed that the saturated solubility of ZrO_2 in the FLiBe melt was 3.84×10^{-3} mol kg^{-1} with equilibrium time of 6 h, and its corresponding apparent solubility product (K'_{sp}) was 3.40×10^{-5} mol^3 kg^{-3}. The interaction between Zr(IV) and O^{2-} was studied by titrating lithium oxide (Li_2O) into the FLiBe melt containing zirconium tetrafluoride (ZrF_4), and the concentration of residual Zr(IV) in the melt gradually decreased due to precipitate formation. The precipitate corresponded to ZrO_2, as confirmed by the stoichiometric ratio and X-ray diffraction analysis. The K'_{sp} was 3.54×10^{-5} mol^3 kg^{-3}, which was highly consistent with that from the dissolution experiment. The obtained K'_{sp} of ZrO_2 was in the same order of magnitude as that of uranium dioxide (UO_2), indicating that a considerable amount of ZrF_4 could inhibit the UO_2 formation when oxide contamination occurred in the melt containing ZrF_4 and uranium tetrafluoride (UF_4). Further oxide titration in the LiF–BeF_2–ZrF_4 (5 mol%)–UF_4 (1.2 mol%) system showed that ZrO_2 was formed first with O^{2-} addition less than 1 mol kg^{-1}, and the precipitation of UO_2 began only after the O^{2-} addition reached 1 mol kg^{-1} and the precipitation of ZrO_2 decreased the ZrF_4 concentration to 0.72 mol kg^{-1} (3 mol%). Lastly, UO_2 and ZrO_2 coprecipitated with further O^{2-} addition of more than 1 mol kg^{-1}. The preferential formation of ZrO_2 effectively avoided the combination of UF_4 and O^{2-}. This study provides a solution for the control of UO_2 precipitation in molten salt reactors.

Received 24th March 2021
Accepted 18th May 2021

DOI: 10.1039/d1ra02332b

rsc.li/rsc-advances

1. Introduction

Molten salt reactors (MSRs) use molten fluoride mixtures, usually lithium fluoride–beryllium fluoride mixed melt (LiF–BeF_2 (2 : 1 mol, FLiBe)) as the carrier solvent of fuel, with uranium tetrafluoride (UF_4) or thorium tetrafluoride (ThF_4) dissolved as fuel salt.[1–3] However, these fluorides can absorb water due to their hygroscopic nature, and pyrohydrolysis commonly occurs upon melting, thus producing an active oxide impurity (O^{2-}) (eqn (1)).[4,5]

$$H_2O + 2F^- = 2HF + O^{2-} \quad (1)$$

Unfortunately, UF_4 has a high sensitivity toward O^{2-} in fluoride melts and forms some insoluble compounds of oxides or oxyfluorides,[6] *e.g.*, uranium dioxide (UO_2) according to our previous investigations (eqn (2)).[7,8]

$$UF_4 + 2O^{2-} = UO_2(s) + 4F^-. \quad (2)$$

The large accumulation of the fuel precipitate UO_2 would generate a superheated area in the reactor and cause a criticality risk.[7–11] Hence, the generation of UO_2 in the fuel salt should be strictly controlled to ensure the safe operation of MSR. Two methods have been proposed to protect uranium from UO_2 precipitate formation. One method is to remove the O^{2-} impurity in the fuel salt before loaded into the reactor, whereas the other approach is to develop feasible additives to collect O^{2-} or facilitate the solubility of UO_2 in molten fluorides during the MSR operation. The Oak Ridge National Laboratory (ORNL) has proposed that bubbling hydrogen fluoride and hydrogen gas (HF/H_2) mixtures into the salt is an effective means to remove O^{2-} (eqn (3)).[12–14]

$$O^{2-} + 2HF(g) = H_2O(g) + 2F^-. \quad (3)$$

However, the HF/H_2 purification method has a limited capacity for oxide removal and cannot totally eliminate the O^{2-} due to the chemical equilibrium. Moreover, the active oxygen still can be produced through the unexpected nuclear reaction and brought by the cover gas and the external environment.[11,12,15] That means, the residual O^{2-} impurity contained in fluorides is inevitable and the formation of UO_2 during the MSR operation remains possible.

[a]*Shanghai Institute of Applied Physics, Chinese Academy of Sciences, Shanghai 201800, PR China. E-mail: huangwei@sinap.ac.cn; Fax: +86 021 39190136; Tel: +86 021 39190136*

[b]*University of Chinese Academy of Sciences, Beijing 100049, PR China*

Therefore, the development of certain feasible additives to timely collect O^{2-} or the improvement of the solubility of UO_2 in the molten fluorides is more effective. Zirconium tetrafluoride (ZrF_4) may be a good selection, which has a strong affinity toward oxide and is a good oxide getter that can easily capture O^{2-} to form zirconium oxides (*e.g.*, ZrO_2) or zirconium oxyfluoride species (*e.g.*, $ZrOF_2$ and $Zr_2OF_{10}^{4-}$) in the molten fluorides.[16,17] In this manner, the combination of U(IV) and O^{2-} can be effectively avoided. Shen *et al.*[16] have studied the interactions between Zr(IV) and O^{2-} in lithium fluoride–sodium fluoride–potassium fluoride (LiF–NaF–KF (46.5 : 11.5 : 42 mol%, FLiNaK)) molten salt and found that different products are formed at different molar ratios of nZr(IV)/$n$$O^{2-}$. ZrO_2 is first formed with nZr(IV)/$n$$O^{2-}$ $\leq$ 0.5, and the formed ZrO_2 redissolves into the melt as $Zr_2OF_{10}^{4-}$ when nZr(IV)/$n$$O^{2-}$ > 0.5. These results indicate that the free oxide ions (O^{2-}) in the melt can be converted into oxyfluoride complex species ($Zr_2OF_{10}^{4-}$) with enough ZrF_4 additive, which further prevents the UO_2 generation successfully. Besides, Gibilaro[18] has found that the addition of calcium oxide (CaO) into a ZrF_4-containing lithium fluoride–calcium fluoride (LiF–CaF_2) salt leads to the formation of a close to equimolar mixture of solid ZrO_2 and $ZrO_{1.3}F_{1.4}$. Korenko *et al.*[19] and our previous studies[7,8,16,20] have used X-ray diffraction (XRD) phase analysis and electrochemical techniques and discovered the ZrO_2 formation when oxide contamination occurs in the ZrF_4-containing systems (*i.e.*, LiF–NaF–KF–ZrF_4 and LiF–NaF–KF–UF_4–ZrF_4), whereas only UO_2 is observed in the systems without ZrF_4 (*i.e.*, LiF–NaF–KF–UF_4 and LiF–BeF_2–UF_4). These studies demonstrate that O^{2-} in zirconium-based systems can be reduced by forming Zr(IV) oxide or oxyfluorides, preventing the UO_2 precipitation.

ZrF_4 can also increase the solubility of oxides because of its strong affinity toward oxygen ions. Song *et al.*[21] have studied the dissolution behavior of chromium sesquioxide (Cr_2O_3) in various molten fluorides and found that the ZrF_4 additive remarkably increases the solubility of Cr_2O_3 by 19 and 2 times in FLiNaK and FLiBe molten salt, respectively, most likely yielding the dissolution product of $[ZrO_xF_y]^{4-2x-y}$ complex species. Peng *et al.*[17] have studied the dissolution–precipitation behaviors of UO_2 in molten fluorides and found that ZrF_4 can also improve the solubility of UO_2. Their results show that the maximum solubility of UO_2 in FLiNaK melt increases by a factor of 5.76 (*i.e.*, increase from 0.247 wt% to 1.422 wt%) when the added ZrF_4 concentration is up to 2.91 wt% and the oxide is dissolved as UOF_2 and $ZrOF_2$ species. These studies demonstrate that ZrF_4 can easily combine with oxygen ions and form soluble Zr(IV)–oxyfluorides to improve the solubility of oxides.

From the above, ZrF_4 is probably an ideal additive for controlling the precipitation of UO_2 in molten fluorides. Moreover, ZrF_4 has a low neutron-absorption cross-section, which allows its use in the fuel of MSR. Based on this finding, ORNL[10,11,22] adopts the LiF–BeF_2–ZrF_4–UF_4 (65 : 29.1 : 5 : 0.9 mol%) as the fuel salt of the molten salt reactor experiment, and the use of 5 mol% ZrF_4 successfully raises the oxide tolerance (the maximum allowable amount of O^{2-} added without the production of UO_2 in the molten salt) to above 100 ppm compared with that of 30 ppm in the molten salt breeder reactor by using a zirconium-free system, *i.e.*, LiF–BeF_2–ThF_4–UF_4 (71.7 : 16 : 12 : 0.3 mol%). At present, the thorium molten salt reactor-liquid fuel (type 1) (TMSR-LF1) program of China is being launched in the Shanghai Institute of Applied Physics, Chinese Academy of Sciences (SINAP@CAS), which also uses a zirconium-containing system composed of LiF–BeF_2–ZrF_4–UF_4 (65.1 : 28.7 : 5 : 1.2 mol%) as the fuel salt.

In this paper, the dissolution–precipitation behaviors of ZrO_2 and the interactions between Zr(IV) and O^{2-} in the FLiBe melt are first studied. Then the apparent solubility product (K'_{sp}) of ZrO_2 is obtained and compared with that of UO_2 to predict the generation of oxide precipitations in the fuel salt containing both UF_4 and ZrF_4. The oxide titration experiment is performed in the FLiBe–ZrF_4 (5 mol%)–UF_4 (1.2 mol%) system, and the evolutions for the equilibrium concentrations of U(IV), Zr(IV), and O^{2-} with oxide additions are studied to further confirm above theoretical prediction. Finally, the inhibiting effect of ZrF_4 on UO_2 formation is further verified. This study provides an effective solution for controlling and monitoring the nuclear fuel precipitation (UO_2) in molten fluorides, which is of great importance for the safe operation of MSR.

2. Experimental

2.1 Molten salt

The highly purified FLiBe (99.9%) eutectic salt with eutectic temperature of 733 K was prepared and supplied by the SINAP@CAS. The received FLiBe eutectic salt was stored in a glovebox and further dehydrated before use by heating under vacuum from ambient temperature to its melting point for 72 h, to guarantee the high-purity of salt and ensure the reliability of the experiments. During this process, the moisture absorbed by the salt was effectively removed. In order to avoid residual HF remaining in FLiBe, the melt was further purified by sparging the ultra-pure H_2 for 8 h. The FLiBe–ZrF_4 and FLiBe–ZrF_4–UF_4 melts were thus prepared by artificially adding ZrF_4 (99.99%; Sigma-Aldrich) and UF_4 (99.99%; China North Nuclear Fuel Co., Ltd) to the prepared FLiBe salt.

2.2 Experimental method

During the dissolution experiments, the excess of powdery ZrO_2 (*ca.* 5 g, 99.99%; Sigma-Aldrich) was manufactured into sheets by tableting. The ZrO_2 sheet was dissolved in 50 g FLiBe melt contained in a vitreous carbon crucible, and the saturated

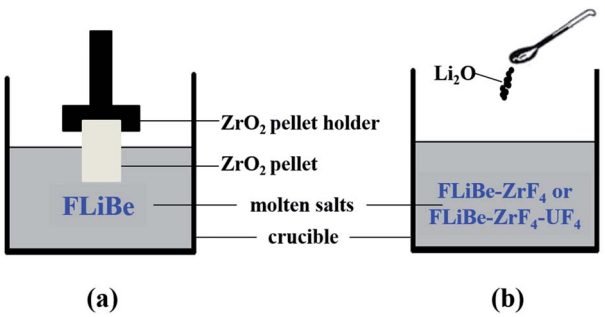

Fig. 1 Schematics of the (a) dissolution and the (b) oxide titration experiments.

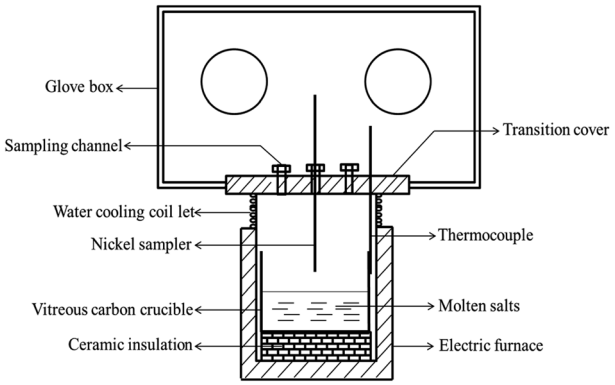

Fig. 2 Schematic of the experimental set-up.

solution of FLiBe–ZrO_2 was formed after equilibrium time. The ZrO_2 sheet was immersed in the salt bath with a graphite pellet holder, as shown in Fig. 1(a). The melt was sampled after the extraction of the pellet from the bath. Thus, no ZrO_2 compound would stick to the sampler, and all the zirconium in the sample was considered to be obtained from ZrO_2 dissolution and could reflect the solubility of ZrO_2.

During the oxide titration experiments, the oxide ions (O^{2-}) were introduced to the FLiBe–ZrF_4 and FLiBe–ZrF_4–UF_4 baths in the form of lithium oxide (Li_2O, 99.99%; Sigma-Aldrich), as shown in Fig. 1(b). The interaction between M(IV) (M = Zr or U) and O^{2-} in the melt would produce ZrO_2 ($\rho = 5.89$ g cm^{-3}) or UO_2 ($\rho = 10.96$ g cm^{-3}) precipitate and gradually deposit to the bottom of the bath ($\rho \approx 2$ g cm^{-3}). When the system reached equilibrium, the supernatant of the molten salt was sampled. The sampling process addressed the use of sintered nickel filter, which prevented the precipitates from sticking to the sampler as proposed by the ORNL,[23] to ensure the accuracy of the experimental results.

The schematic of the experimental apparatus used in present study was shown in Fig. 2, which was described in detail in our previous studies.[7,8,16,17,20,21,24] The whole experiment was conducted in a glove box protected by dry argon atmosphere (99.999%), and the oxygen and water contents in the glove box were both strictly controlled below 0.5 ppm.

2.3 Analytical techniques

The oxide concentration in molten fluorides was determined using the LECO oxygen detector (RO600, LECO Co., Ltd) through the carbothermal reduction technique, which was in accordance with the work of Mediaas[25,26] and our previous studies.[7,8,16,20] Herein, the result measured by LECO was the total oxide content including O^{2-} and oxide in oxygenated anions. The oxygenated anions in the melts were determined using ICE ion chromatography (IC, ICS-2100, Dionex Co., Ltd.) with a valve-switching technology.[8]

The concentration of Zr(IV) or U(IV) ions in molten fluorides was determined using inductively coupled plasma optical emission spectroscopy (ICP-OES, Arcos, Spectro Co., Ltd). The detailed testing process has been described previously.[7,8,17] The oxide precipitates formed in molten salt were analyzed using the XRD technique (DY3614, PANzlytical Co., Ltd).

3. Results

3.1 Concentration of free oxide ions (O^{2-}) in molten fluorides

The oxygen in fluoride salt exists in two forms: (i) free oxide ions (O^{2-}) and (ii) oxygenated anions (*e.g.*, SO_4^{2-}, NO_3^-, and PO_4^{3-}). However, only O^{2-} could form oxide precipitates (*e.g.*, UO_2 and ZrO_2) due to its high sensitivity toward UF_4 and ZrF_4 in molten fluorides. Therefore, the O^{2-} concentration in molten fluorides should be measured to clarify the dissolution–precipitation behavior of the fuel salt for MSR. The practical O^{2-} concentration ($[O^{2-}]$) in molten fluorides was determined by subtracting the oxide concentration in oxygenated anions ($[O]_{IC}$) from the total oxide concentration ($[O]_{LECO}$), as shown in eqn (4). Table 1 gives the oxide analysis results of two batches of FLiBe melts used in the present study. As shown in Table 1, the total oxygen content of 1# FLiBe was 145 ppm, and the oxygenated anions included NO_3^-, SO_4^{2-}, and PO_4^{3-} with content of 83, 55, and 6 ppm, respectively. According to the mass proportion of oxide in the oxygenated anion, the oxide concentrations in NO_3^-, SO_4^{2-}, and PO_4^{3-} were 64, 37, and 4 ppm, respectively. Thus, the sum of oxide concentration in these three oxygenated anions were up to 105 ppm, and the O^{2-} content was 40 ppm in accordance with eqn (4). Likewise, the O^{2-} content of 2# FLiBe was 1383 ppm.

$$[O^{2-}] = [O]_{LECO} - [O]_{IC}. \quad (4)$$

Table 1 Oxide analysis results of the FLiBe melts used in the present study

Batch number of FLiBe	Total oxide concentration ($[O]_{LECO}$)/ppm	Oxygenated anion concentration/ppm		Oxide in oxygenated anions ($[O]_{IC}$)/ppm	O^{2-} concentration ($[O^{2-}]$)/ppm
1# (for oxide titration experiment)	145	NO_3^-	83	105	40 (2.5×10^{-3} mol kg^{-1})
		SO_4^{2-}	55		
		PO_4^{3-}	6		
2# (for dissolution experiment)	1500	NO_3^-	135	117	1383 (8.64×10^{-2} mol kg^{-1})
		SO_4^{2-}	19		
		PO_4^{3-}	—		

3.2 K'_{sp} of ZrO_2

3.2.1 Dissolution method: FLiBe–ZrO_2 system. The ZrO_2 pellet was immersed into the FLiBe melt to determine the solubility of ZrO_2 in this melt. The melt was sampled at different holding times at 873 K, and the Zr(IV) concentration in each sample was measured. Fig. 3 gives the plots of Zr(IV) concentration in the melt *versus* the dissolution time of ZrO_2. Apparently, the initial zirconium concentration in the FLiBe melt was below the detection limit of ICP-OES (<0.01 ppm or 1×10^{-7} mol kg^{-1}) and could not be detected. When the ZrO_2 was dissolved for the first 2 h, the Zr(IV) concentration remarkably increased to 3.37×10^{-3} mol kg^{-1}. Afterwards, the growth rate of Zr(IV) concentration slowed down, and its value gradually increased to 3.84×10^{-3} mol kg^{-1} when the dissolution time further increased to 6 h. Then, no remarkable difference was observed in the results of samples collected from 6 h to 22 h, and the Zr(IV) concentration finally maintained at approximately 3.84×10^{-3} mol kg^{-1}, which corresponded to the solubility of ZrO_2 with an equilibrium time of 6 h.

In the FLiBe–ZrO_2 system, when the dissolution equilibrium of ZrO_2 was achieved, the substances of ZrO_2 compound, Zr(IV), and O^{2-} ions, coexisted and equilibrated, as shown in eqn (5). Thus, the real solubility product (K_{sp}) of ZrO_2 could be obtained by multiplying the equilibrium activity of Zr(IV) ($a_{Zr(IV)}$) and O^{2-} ($a_{O^{2-}}$), as shown in eqn (6). Actually, a certain deviation existed between the activity (a) and the apparent concentration, and this deviation could be quantitatively expressed using the activity coefficient (γ) with the value less than 1, as shown in eqn (7) and (8). In fact, the [Zr(IV)] and $[O^{2-}]$ values obtained by ICP-OES, LECO, and IC techniques were the results of apparent concentrations. Thus, the real solubility product (K_{sp}) of ZrO_2 could be calculated through eqn (6), where K'_{sp} is the apparent solubility product that can be obtained using experimental methods, as shown in eqn (9). However, the measurement of a and γ (γ_1 for Zr(IV) and γ_2 for O^{2-}, which can be considered as constant in this case) in molten fluorides is a challenging task and leads to a difficult determination of the real K_{sp}. Nevertheless, the present study only considered the apparent concentration to deal with this issue, and the K'_{sp} calculation could also make sense in case of apparent concentration consideration (eqn (9)).

$$ZrO_2(s) \leftrightarrow Zr(IV) + 2O^{2-}. \quad (5)$$

$$K_{sp} = a_{Zr(IV)} \cdot (a_{O^{2-}})^2 = \gamma_1\gamma_2^2 \cdot [Zr(IV)][O^{2-}]^2 = \gamma_1\gamma_2^2 \cdot K'_{sp}. \quad (6)$$

$$a_{Zr(IV)} = \gamma_1 \cdot [Zr(IV)]. \quad (7)$$

$$a_{O^{2-}} = \gamma_2 \cdot [O^{2-}]. \quad (8)$$

$$K'_{sp} = [Zr(IV)][O^{2-}]^2. \quad (9)$$

$$[O^{2-}] = [O^{2-}]_{ZrO_2} + [O^{2-}]_{FLiBe}. \quad (10)$$

$$[O^{2-}]_{ZrO_2} = 2[Zr(IV)]. \quad (11)$$

Then, the equilibrium [Zr(IV)] and $[O^{2-}]$ were measured to determine the value of K'_{sp}. In accordance with the solubility of ZrO_2 in FLiBe, as shown in Fig. 3, the equilibrium [Zr(IV)] in the bath was 3.84×10^{-3} mol kg^{-1}, whereas the O^{2-} concentration caused by ZrO_2 dissolution ($[O^{2-}]_{ZrO_2}$) was twice of the [Zr(IV)], *i.e.*, 7.68×10^{-3} mol kg^{-1} (eqn (5) and (11)). Besides, the initial O^{2-} content in the FLiBe melt ($[O^{2-}]_{FLiBe}$) was 8.64×10^{-2} mol kg^{-1} (1383 ppm, Table 1). Thus, the equilibrium $[O^{2-}]$ was 9.41×10^{-2} mol kg^{-1}, which was obtained using the sum of $[O^{2-}]_{ZrO_2}$ and $[O^{2-}]_{FLiBe}$ (eqn (10)). Then, with the obtained values of [Zr(IV)] and $[O^{2-}]$, the K'_{sp} was calculated to be 3.40×10^{-5} mol^3 kg^{-3} (eqn (9)).

3.2.2 Oxide titration method: FLiBe–ZrF_4–Li_2O system. Oxide ions in the form of Li_2O were gradually added to the FLiBe–ZrF_4 (5 mol%) melt to investigate the interaction between Zr(IV) and O^{2-} and its corresponding product. Then, the supernatant melt was sampled after the system reached equilibrium at 873 K, and the Zr(IV) concentration in each sample was analyzed. Table 2 shows the variation of Zr(IV) concentration with different oxide additions at 873 K. Apparently, the residual Zr(IV) concentration in the melt linearly decreased with increasing oxide addition, and the slope of this fitted straight line was 0.51, which approximately equaled to 0.5, as shown in Fig. 4. This result meant a zirconium-containing precipitate with the stoichiometry of $1Zr^{4+}$:$2O^{2-}$, probably ZrO_2 or $Zr_xO_{2x}F_y$ species, was formed. Moreover, a kind of white precipitate at the

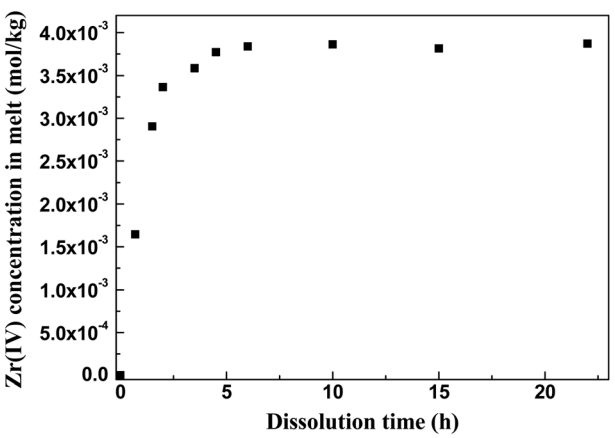

Fig. 3 Zr(IV) concentration *versus* the dissolution time of ZrO_2 in the FLiBe melt at 873 K.

Table 2 Residual Zr(IV) and O^{2-} concentrations in the FLiBe–ZrF_4 (5 mol%) melt with different oxide additions, and the variation of calculated K'_{sp} (ZrO_2) value (equilibrium time: 10 h; temperature: 873 K)

Added O^{2-} (mol kg^{-1})	Equilibrium [Zr(IV)] in melt (mol kg^{-1})	Equilibrium $[O^{2-}]$ in melt (mol kg^{-1})	K'_{sp} of ZrO_2 (mol^3 kg^{-3})
0	1.33	—	—
0.11	1.29	5.20×10^{-3} (83 ppm)	3.49×10^{-5}
0.16	1.27	5.29×10^{-3} (85 ppm)	3.55×10^{-5}
0.26	1.23	5.43×10^{-3} (87 ppm)	3.63×10^{-5}
0.34	1.18	5.48×10^{-3} (88 ppm)	3.54×10^{-5}
0.47	1.08	5.71×10^{-3} (91 ppm)	3.52×10^{-5}

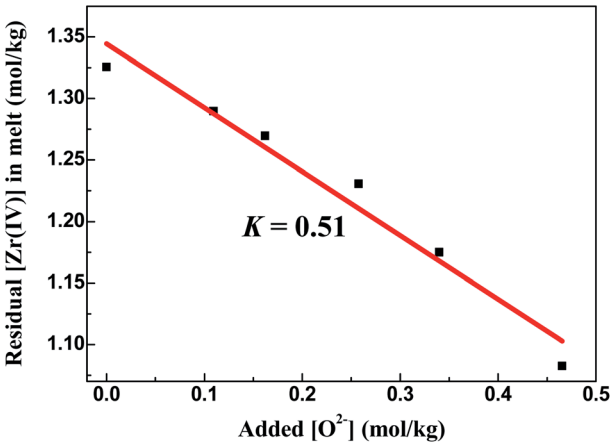

Fig. 4 Linear relationship between the residual [Zr(IV)] and the added $[O^{2-}]$ in the FLiBe–ZrF_4 (5 mol%) melt at 873 K.

bottom of the melting bath was observed during oxide titration, as shown in Fig. 5(a). To identify the precipitated species, the bottom precipitate was sampled, distilled (to remove the residual matrix salt) and further transferred for XRD analysis.

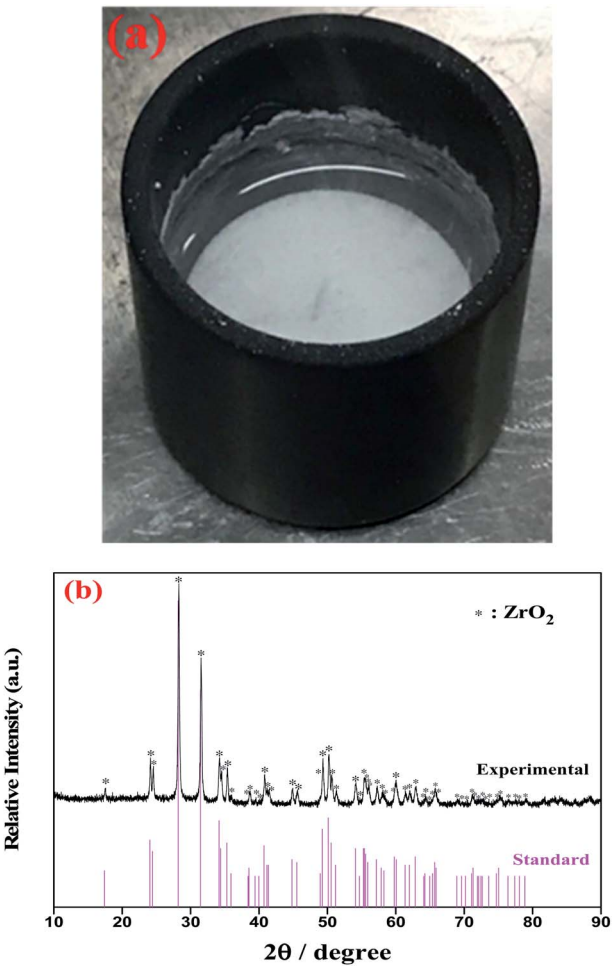

Fig. 5 (a) The observed white precipitate formed at the bottom of the FLiBe–ZrF_4 (5 mol%) melt with O^{2-} addition at 873 K. (b) XRD pattern of this precipitate obtained after distillation treatment.

The result confirmed that this precipitate corresponded to ZrO_2, as shown in Fig. 5(b).

With the formation of ZrO_2, its K'_{sp} could be calculated by multiplying the equilibrium concentration of O^{2-} by Zr(IV) (eqn (9)). As shown in Table 2, when the added O^{2-} increased from 0 mol kg^{-1} to 0.47 mol kg^{-1}, the remaining Zr(IV) in the melt gradually decreased from 1.33 mol kg^{-1} to 1.08 mol kg^{-1} whereas the equilibrium O^{2-} concentration increased from 5.20×10^{-3} mol kg^{-1} to 5.71×10^{-3} mol kg^{-1}. Thus, a set of K'_{sp} values were obtained respectively during each oxide addition, and the results located within $(3.49–3.63) \times 10^{-5}$ mol^3 kg^{-3}. The slight variation in the K'_{sp} may be attributed to the testing error caused by the chemical analysis. The eqn (9) could be written as:

$$[Zr(IV)] = K'_{sp} \cdot \frac{1}{[O^{2-}]^2}. \quad (12)$$

The linear relationship between the residual [Zr(IV)] and $1/[O^{2-}]^2$ was fitted (Fig. 6), and the slope of this straight line corresponded to the statistical result of K'_{sp}. Thus, the final result of K'_{sp} was determined to be 3.54×10^{-5} mol^3 kg^{-3}. This value was highly consistent with that obtained by the dissolution method in FLiBe–ZrO_2 system (3.40×10^{-5} mol^3 kg^{-3}), as stated in Sect. 3.2.1.

3.3 Oxide titration to the molten FLiBe–ZrF_4–UF_4 system

Oxide ions in the form of Li_2O were gradually added to the FLiBe–ZrF_4 (5 mol%)–UF_4 (1.2 mol%) melt to investigate the inhibiting effect of ZrF_4 on UO_2 formation. Then, the evolutions of the equilibrium concentrations of Zr(IV), U(IV), and O^{2-} in the melt with oxide addition were determined, and the results could be shown in two stages, as shown in Fig. 7.

3.3.1 Stage 1: ZrO_2 formation (O^{2-} addition <1 mol kg^{-1}). The initial Zr(IV) and U(IV) contents of the molten salt were 5 mol% (1.21 mol kg^{-1}) and 1.2 mol% (0.28 mol kg^{-1}), respectively. Before the added O^{2-} reached 1 mol kg^{-1}, the residual

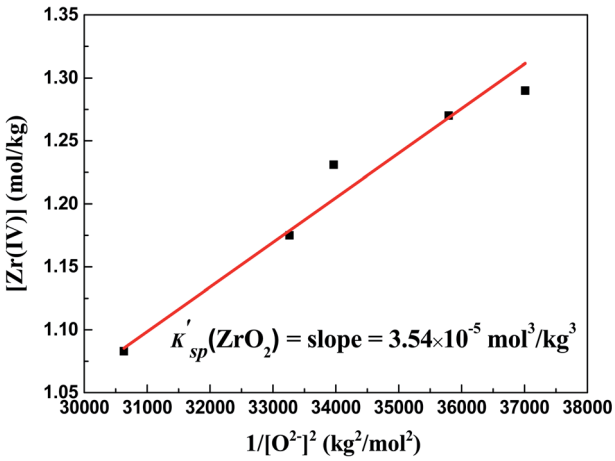

Fig. 6 Determination of K'_{sp} (ZrO_2) in the FLiBe–ZrF_4 (5 mol%) melt with O^{2-} additions at 873 K: linear relationship between the residual [Zr(IV)] and $1/[O^{2-}]^2$.

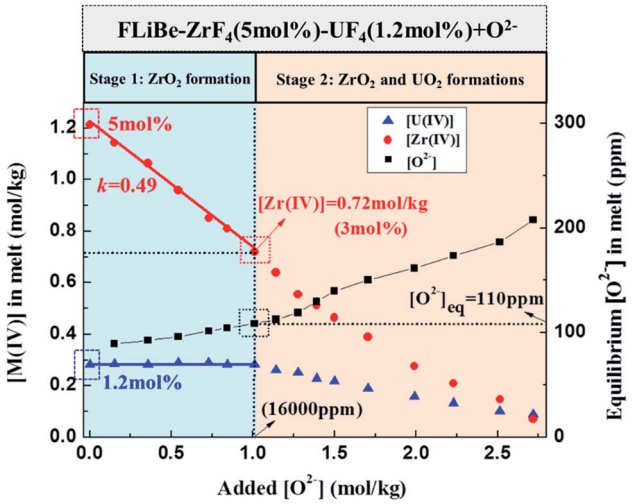

Fig. 7 Evolutions of the equilibrium [Zr(IV)], [U(IV)], and [O^{2-}] in the FLiBe–ZrF_4 (5 mol%)–UF_4 (1.2 mol%) melt with oxide additions at 873 K.

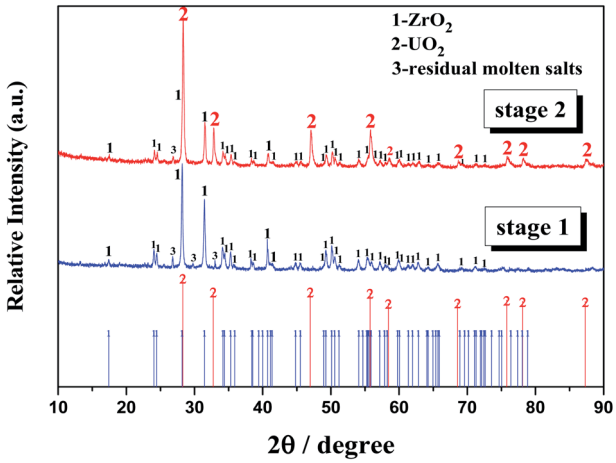

Fig. 8 XRD patterns of the bottom samples obtained in the FLiBe–ZrF_4 (5 mol%)–UF_4 (1.2 mol%) melt with oxide additions after distillation treatment. Stage 1: oxide addition <1 mol kg^{-1}; stage 2: oxide addition >1 mol kg^{-1}.

Zr(IV) concentration in melt linearly decreased to 0.72 mol kg^{-1} and the U(IV) concentration almost remained invariable, whereas the equilibrium O^{2-} increased from 90 ppm to 110 ppm. This result indicated that only zirconium-containing precipitate was formed in this period. The slope of the linear relationship between the residual [Zr(IV)] and the added [O^{2-}] (0–1 mol kg^{-1}) was fitted as 0.49, which approximately equaled to 0.5 (Fig. 7), presuming that insoluble ZrO_2 or $Zr_xO_{2x}F_y$ species was formed in the melt. Moreover, a kind of white precipitate was observed at the bottom of the bath during experiment, and XRD analysis further proved that this precipitate corresponded to ZrO_2 (Fig. 8). Therefore, only ZrO_2 precipitate was formed with oxide addition less than 1 mol kg^{-1}.

3.3.2 Stage 2: ZrO_2 and UO_2 formations (O^{2-} addition ≥1 mol kg^{-1}). When the added O^{2-} reached 1 mol kg^{-1}, the U(IV) concentration drop began, and the equilibrium O^{2-} at this time was 110 ppm. When the added O^{2-} exceeded 1 mol kg^{-1} and reached 2.72 mol kg^{-1}, the Zr(IV) and U(IV) in melt were simultaneously consumed and finally decreased to 0.07 and 0.09 mol kg^{-1}, respectively. Meanwhile the equilibrium O^{2-} further increase to 208 ppm. These results indicated that both zirconium-containing and uranium-containing precipitates were formed in this stage. In addition, the stoichiometry of the total reacted metal ions M(IV) (M = Zr or U) and the added O^{2-} was approximately 1 : 2 during this stage. After completion of the experiment, two kinds of precipitates were observed at the bottom of salt. The white one corresponded to ZrO_2 and the rufous one corresponded to UO_2, as confirmed by XRD (Fig. 8). Therefore, both ZrO_2 and UO_2 were formed with oxide addition more than 1 mol kg^{-1}.

4. Discussion

4.1 K'_{sp}: analysis of oxide precipitation behavior in the FLiBe melt

The K'_{sp} of ZrO_2 and UO_2 in FLiBe melt were compared to clarify the precipitation law of these two oxides. According to our previous investigation,[8] the K'_{sp} (UO_2) in the FLiBe melt obtained using the dissolution and the oxide titration methods at 873 K were 1.67 × 10^{-5} and 1.33 × 10^{-5} mol^3 kg^{-3}, respectively. In this work, the K'_{sp} (ZrO_2) using the dissolution and the oxide titration methods at 873 K were 3.40 × 10^{-5} and 3.54 × 10^{-5} mol^3 kg^{-3}, respectively. As an equilibrium constant, the K_{sp} theoretically depended on temperature only, and the present results also agreed well with those reported by ORNL at the same temperature,[22] as summarized in Table 3.

Evidently, K'_{sp} (ZrO_2) and K'_{sp} (UO_2) were in the same order of 10^{-5} mol^3 kg^{-3}, and K'_{sp} (ZrO_2) was 2–3 times higher than K'_{sp} (UO_2). Based on these results, we can predict the formation of ZrO_2 and UO_2 precipitates in the FLiBe melt. (i) When the FLiBe melt only contained UF_4, the reactive oxide resulted in UO_2 precipitation. (ii) When the FLiBe melt contained equimolar ZrF_4 and UF_4, the oxide contamination should first yield the UO_2 precipitate. (iii) In addition, when the FLiBe melt contained considerably more ZrF_4 than UF_4, the oxide contamination should first yield the ZrO_2 precipitate. The precipitation of UO_2 began only after the precipitation of ZrO_2 had dropped the ZrF_4 concentration to near 2–3 times as high as that of UF_4. With further oxide addition, UO_2 and ZrO_2 would precipitate simultaneously. Therefore, excessive ZrF_4 with more than 3 times higher than UF_4 can effectively avoid the formation of UO_2 precipitate in the FLiBe melt.

4.2 Oxide precipitation behavior of the MSR fuel salt system FLiBe–ZrF_4–UF_4

The oxide titration experiment in the FLiBe–ZrF_4–UF_4 melt with considerably more ZrF_4 than UF_4 was conducted to validate the above theoretical prediction and further clarify the influence of ZrF_4 on UO_2 generation, as shown in Fig. 7. At first, the ZrF_4 in the system was consumed by forming ZrO_2, thereby protecting uranium from being precipitated. Until the ZrF_4 concentration dropped to 0.72 mol kg^{-1} (3 mol%), precipitation of UO_2 began to form. At this point, the Zr(IV) concentration was about 2.5

Table 3 Comparison between K'_{sp} (ZrO_2) and K'_{sp} (UO_2) and their ratio K'_{sp} (ZrO_2)/K'_{sp} (UO_2) (k) in the FLiBe melt at 873 K

	K'_{sp} by dissolution method (mol^3 kg^{-3})	K'_{sp} by oxide titration method (mol^3 kg^{-3})	K_{sp} reported by ORNL[22] (mol^3 kg^{-3})
ZrO_2	3.40×10^{-5}	3.54×10^{-5}	3.20×10^{-5}
UO_2	1.67×10^{-5} (ref. 8)	1.33×10^{-5} (ref. 8)	1.20×10^{-5}
k	2.04	2.66	2.67

times as high as that of U(IV). This result was highly consistent with the theoretical prediction, as stated in Sect. 4.1.

With the measured equilibrium concentrations of M(IV) (M = Zr or U) and O^{2-}, a set of K'_{sp} values for ZrO_2 and UO_2 could be respectively obtained after each oxide addition, as shown in Table 4. The K'_{sp} results were basically consistent with that obtained in the FLiBe melt (Table 3) but varied with O^{2-} addition. This was caused by the concentration change of M(IV) in the melt. The K'_{sp} (ZrO_2) showed no great difference when the added O^{2-} was less than 1.71 mol kg^{-1}, but decreased from 3.45×10^{-5} mol^3 kg^{-3} to 1.19×10^{-5} mol^3 kg^{-3} when the added O^{2-} further increased from 1.71 mol kg^{-1} to 2.72 mol kg^{-1}. At this time, the concentration of Zr(IV) was below 0.39 mol kg^{-1}. Whereas the K'_{sp} (UO_2) had no remarkable change except some slight fluctuations. The variation of K'_{sp} (ZrO_2) probably arose from the deviation between the apparent concentration (c) and the activity (a) for Zr(IV) in the melt, as shown in eqn (7). The extent of this deviation ($\gamma \leq 1$) was correlated to the concentration of ions. γ increased and decreased when the solute concentration decreased and increased, respectively. In this case, the initial Zr(IV) concentration was about four times greater than the initial U(IV) concentration, and the decrement in [Zr(IV)] varied in a wide range during oxide titration. Thus, when the residual Zr(IV) concentration continued decreasing to a low extent (the added O^{2-} was more than 1.71 mol kg^{-1} and [Zr(IV)] was below 0.39 mol kg^{-1}, which was 1/3 of the initial one), the γ_1 for Zr(IV) would increase. Meanwhile, [O^{2-}] changed slightly (only about 100 ppm change), indicating that γ_2 for O^{2-} remained virtually unchanged. According to eqn (6) and (9), the calculated K'_{sp} (ZrO_2) gradually decreased under low [Zr(IV)] when the added O^{2-} was more than 1.71 mol kg^{-1} and [Zr(IV)] was below 0.39 mol kg^{-1}. With regard to U(IV), whose concentration still stayed at a relatively low level, and the decrement occurred on a smaller scale compared with that of Zr(IV). Herein, the $\gamma_{U(IV)}$ might change slightly, so did the γ_2 for O^{2-}. Thus, no remarkable variation in K'_{sp} (UO_2) was observed in the whole oxide titration procedure.

Fig. 9 illustrates the evolution of K'_{sp} (ZrO_2)/K'_{sp} (UO_2) ratio (k) in the oxide titration duration. The k value was also equal to the ratio of [Zr(IV)]/[U(IV)] because the O^{2-} was simultaneously equilibrated by ZrO_2 and UO_2, as shown in eqn (13). Apparently, K'_{sp} (ZrO_2) was 2.54–1.46 times greater than K'_{sp} (UO_2) when the added O^{2-} was in the range of 1.01–2.51 mol kg^{-1}. However, the difference between them narrowed (decreasing k) with oxide addition, and K'_{sp} (ZrO_2) < K'_{sp} (UO_2) happened when the oxide addition reached 2.72 mol kg^{-1} (Fig. 9, bottom X-axis). Meanwhile, the decrease in [Zr(IV)]/[U(IV)] ratio with decreasing uranium concentration was also found (Fig. 9, top X-axis). These results reveal two important information: (i) proposing a solution for monitoring the generation of UO_2 by measuring the k value in the melt with known [U(IV)]. For example, in this case the FLiBe–ZrF_4 (5 mol%)–UF_4 (1.2 mol%) melt, as long as k > 2.5, namely the Zr(IV) concentration remains more than 2.5 times that of U(IV), the oxide contamination will not cause UO_2 precipitation; (ii) when [U(IV)] is different, the required [Zr(IV)] (actually, the ratio of [Zr(IV)]/[U(IV)], k) which can prevent UO_2

Table 4 Variation in K'_{sp} for ZrO_2 and UO_2 in the FLiBe–ZrF_4 (5 mol%)–UF_4 (1.2 mol%) melt with oxide addition at 873 K

Added [O^{2-}] (mol kg^{-1})	[O^{2-}] (mol kg^{-1})	[Zr(IV)] (mol kg^{-1})	[U(IV)] (mol kg^{-1})	K'_{sp} (ZrO_2) (mol^3 kg^{-3})	K'_{sp} (UO_2) (mol^3 kg^{-3})
0.15	5.59×10^{-3} (89 ppm)	1.14	0.29	3.57×10^{-5}	— (no UO_2 formed)
0.36	5.79×10^{-3} (93 ppm)	1.06	0.28	3.56×10^{-5}	— (no UO_2 formed)
0.54	6.01×10^{-3} (96 ppm)	0.96	0.29	3.47×10^{-5}	— (no UO_2 formed)
0.73	6.35×10^{-3} (102 ppm)	0.85	0.29	3.43×10^{-5}	— (no UO_2 formed)
0.84	6.53×10^{-3} (105 ppm)	0.81	0.28	3.46×10^{-5}	— (no UO_2 formed)
1.01	6.80×10^{-3} (109 ppm)	0.72	0.28	3.33×10^{-5}	1.31×10^{-5}
1.14	7.03×10^{-3} (113 ppm)	0.64	0.26	3.16×10^{-5}	1.30×10^{-5}
1.28	7.44×10^{-3} (119 ppm)	0.55	0.25	3.07×10^{-5}	1.40×10^{-5}
1.39	8.10×10^{-3} (130 ppm)	0.51	0.23	3.36×10^{-5}	1.50×10^{-5}
1.50	8.73×10^{-3} (140 ppm)	0.46	0.22	3.53×10^{-5}	1.66×10^{-5}
1.71	9.40×10^{-3} (150 ppm)	0.39	0.19	3.45×10^{-5}	1.68×10^{-5}
1.99	1.01×10^{-2} (161 ppm)	0.28	0.16	2.81×10^{-5}	1.61×10^{-5}
2.23	1.08×10^{-2} (173 ppm)	0.21	0.13	2.47×10^{-5}	1.56×10^{-5}
2.51	1.17×10^{-2} (186 ppm)	0.15	0.10	1.99×10^{-5}	1.36×10^{-5}
2.72	1.30×10^{-2} (208 ppm)	0.07	0.09	1.19×10^{-5}	1.50×10^{-5}

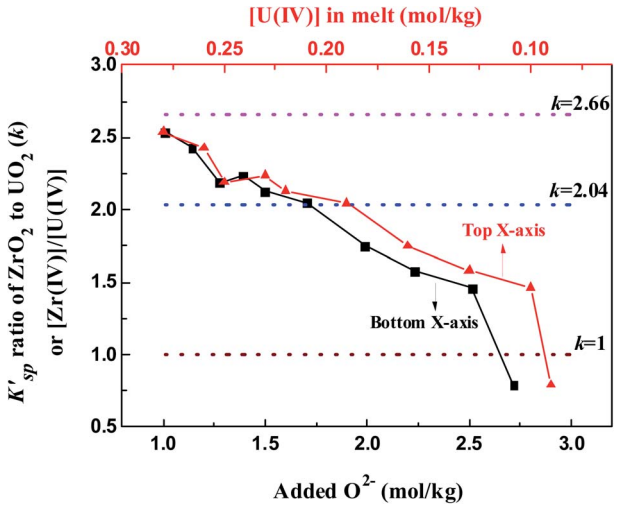

Fig. 9 K'_{sp} ratio of ZrO_2 to UO_2 (k) during the oxide titration of FLiBe–ZrF_4 (5 mol%)–UF_4 (1.2 mol%) melt at 873 K. $k = 2.66$ obtained by oxide titration method; $k = 2.04$ obtained by dissolution method; $k = 1$ means K'_{sp} (ZrO_2) = K'_{sp} (UO_2).

precipitation also changes. The lower the [U(IV)] is, the lower the required k value will be. For example, when [U(IV)] is 0.29 mol kg^{-1}, $k \geq 2.5$ is needed to prevent UO_2 precipitation. However, when [U(IV)] is 0.09 mol kg^{-1}, it only requires $k \geq 0.8$. That means the required [Zr(IV)] decreased with decreasing [U(IV)]. These results provide reference data for fuel salt design of MSR with different uranium content.

$$k = \frac{K'_{sp}(ZrO_2)}{K'_{sp}(UO_2)} = \frac{[Zr(IV)][O^{2-}]^2}{[U(IV)][O^{2-}]^2} = \frac{[Zr(IV)]}{[U(IV)]} \quad (13)$$

5. Conclusion

The formation of the UO_2 precipitate would lead to a superheated area in MSR and cause a critical risk. Developing appropriate additives for oxide ion capture is an effective way to protect uranium from forming the UO_2 precipitate in the fuel of MSR. This study focused on the dissolution–precipitation behavior of ZrO_2 in the FLiBe melt, and the inhibition of UO_2 generation by the ZrF_4 additive was also clarified.

First, the results of the dissolution experiment showed that the saturated solubility of ZrO_2 in the FLiBe melt at 873 K was 3.84 mol kg^{-1} with the equilibrium time of 6 h. Then, the interactions between Zr(IV) and oxide ions was studied by adding O^{2-} into the FLiBe–ZrF_4 melt. The Zr(IV) concentration in the melt linearly decreased with O^{2-} addition because of ZrO_2 precipitation, which was confirmed by the stoichiometric ratio (chemical analysis) and XRD. Moreover, the K'_{sp} of ZrO_2 were determined to be 3.40×10^{-5} and 3.54×10^{-5} mol^3 kg^{-3} in these two processes, which showed good conformity and were highly consistent with that reported by ORNL.

The obtained K'_{sp} of ZrO_2 was in the same order of 10^{-5} mol^3 kg^{-3} and 2–3 times higher than that of UO_2. Based on this result, the formation of ZrO_2 and UO_2 precipitates in the FLiBe melt can be predicted. If the FLiBe melt contained considerably more ZrF_4 than UF_4, the oxide contamination first yielded the ZrO_2 precipitate, and the precipitation of UO_2 began only when the precipitation of ZrO_2 had dropped the ZrF_4 concentration to near 2–3 times as high as that of UF_4. The oxide titration experiment of the FLiBe–ZrF_4 (5 mol%)–UF_4 (1.2 mol%) melt was further carried out, showing that only ZrO_2 was formed when the O^{2-} addition was less than 1 mol kg^{-1}. When the added O^{2-} reached 1 mol kg^{-1} and the [Zr(IV)] reduced to 0.72 mol kg^{-1} (3 mol%), UO_2 began to form and the [Zr(IV)]/[U(IV)] ratio was 2.5 at this point. Afterwards, ZrO_2 and UO_2 coprecipitated with further O^{2-} addition. Experimental results agreed well with the theoretical prediction from the obtained K'_{sp} (ZrO_2) and K'_{sp} (UO_2).

The results of present work clarified the inhibiting effect of ZrF_4 on the UO_2 generation in the FLiBe melt and further affirmed the approach of ZrF_4 additive for the control of nuclear fuel precipitation (UO_2) in MSR. When oxide contamination occurred, the considerable amount of ZrF_4 first formed ZrO_2, which prevented the combination between UF_4 and O^{2-}. Thus, the precipitation of UO_2 could be effectively avoided. The critical ratio of [Zr(IV)]/[U(IV)] to prevent the precipitation of UO_2 was more than 2.5 in the FLiBe–ZrF_4 (5 mol%)–UF_4 (1.2 mol%) melt, and it decreased with decreasing initial uranium concentration. The precipitation mechanism of ZrO_2 and UO_2 in the FLiBe molten salt can provide the following inspirations: (i) a solution for monitoring the generation of UO_2 precipitation in the MSR fuel salt can be proposed by measuring the [Zr(IV)]; (ii) the required [Zr(IV)]/[U(IV)] ratio which can prevent UO_2 precipitation changes with different uranium content. All of these will be helpful for the safe operation and fuel salt design of MSR.

Conflicts of interest

There are no conflicts to declare.

Acknowledgements

This work was supported by the National Natural Science Foundation of China (Grant No. 22006150), Shanghai Sailing Program (Grant No. 19YF1458200), "Strategic Priority Research Program" and the "Frontier Science Key Program" of the Chinese Academy of Sciences (Grant No. XDA02030000 and QYZDYSSW-JSC016).

References

1 M. Rosenthal, P. Kasten and R. Briggs, Molten-salt reactorsd history, status, and potential, *Nucl. Appl. Technol.*, 1970, **8**, 107–117.
2 W. R. Grimes, F. F. Blankenship, G. W. Keilholtz, H. F. Poppendiek and M. T. Robinson, Chemical aspects of molten fluoride reactors, in *Progress in Nuclear Energy, Series IV*, Pergamon Press, London, 1960, vol. 2.

3 A. Nuttin, D. Heuer, A. Billebaud, R. Brissot, C. Le Brun, E. Liatard, J.-M. Loiseaux, L. Mathieu, O. Meplan and E. Merle-Lucotte, Potential of thorium molten salt reactors: detailed calculations and concept evolution with a view to large scale energy production, *Prog. Nucl. Energy*, 2005, **46**, 77–99.

4 F. Lantelme and H. Groult, *Molten Salts Chemistry: from Lab to Applications*, Elsevier, 2013.

5 S. Delpech, C. Cabet, C. Slim and G. S. Picard, Molten fluorides for nuclear applications, *Mater. Today*, 2010, **13**, 34–41.

6 P. A. Haas and P. Cooper, Solubility of uranium oxides in fluoride salts at 1200 °C, *J. Chem. Eng. Data*, 1993, **38**, 26–30.

7 H. Peng, M. Shen, Y. Zuo, X. X. Tang, R. Tang and L. D. Xie, Electrochemical technique for detecting the formation of uranium-containing precipitates in molten fluorides, *Electrochim. Acta*, 2016, **222**, 1528–1537.

8 H. Peng, W. Huang, L. D. Xie and Q. N. Li, Solubility and precipitation investigations of UO_2 in LiF–BeF_2 molten salt, *J. Nucl. Mater.*, 2020, **531**, 152004.

9 ORNL-3812, *Molten-salt Reactor Program: Semiannual Progress Report for Period Ending*, Oak Ridge National Laboratory, 1965.

10 ORNL-3936, *Molten-salt Reactor Program: Semiannual Progress Report for Period Ending*, Oak Ridge National Laboratory, 1966.

11 ORNL-4812, *Molten-salt Reactor Program: the Development Status of Molten-Salt Breeder Reactors*, Oak Ridge National Laboratory, 1972.

12 ORNL-3708, *Molten-salt Reactor Program: Semiannual Progress Report for Period Ending*, Oak Ridge National Laboratory, 1964.

13 ORNL-4616, *Reactor Chemistry Division: Preparation and Handling of Salt Mixtures for the Molten Salt Reactor experiment*, Oak Ridge National Laboratory, 1971.

14 A. L. Mathews and C. F. Baes Jr., Oxide chemistry and thermodynamics of molten lithium fluoride-beryllium fluoride solutions, *Inorg. Chem.*, 1968, **7**, 373–382.

15 ORNL-TM-0728, *report, MSRE Design and Operations Report: Part I. Description of Reactor Design*, Oak Ridge National Laboratory, 1965.

16 M. Shen, H. Peng, M. Ge, C. Y. Wang, Y. Zuo and L. D. Xie, Chemical interactions between zirconium and free oxide in molten fluorides, *RSC Adv.*, 2015, **5**, 40708–40713.

17 H. Peng, M. Shen, Y. Zuo, H. Y. Fu and L. D. Xie, Chemical and electrochemical studies on the solubility of UO_2 in molten FLINAK with ZrF_4 additive, *J. Nucl. Mater.*, 2018, **510**, 256–264.

18 M. Gibilaro, L. Massot, P. Chamelot, L. Cassayre and P. Taxil, Investigation of Zr(IV) in LiF–CaF_2: stability with oxide ions and electroreduction pathway on inert and reactive electrodes, *Electrochim. Acta*, 2013, **95**, 185–191.

19 M. Korenko, M. Straka, J. Uhlíř, L. Szatmáry, M. Ambrová and M. Šimurda, Phase analysis of the solidified KF–(LiF–NaF–UF_4)–ZrF_4 molten electrolytes for the electrowinning of uranium, *J. Radioanal. Nucl. Chem.*, 2014, **302**, 549–554.

20 M. Shen, H. Peng, M. Ge, Y. Zuo and L. D. Xie, Use of square wave voltammeter for online monitoring of O^{2-} concentration in molten fluorides at 600 °C, *J. Electroanal. Chem.*, 2015, **748**, 34–39.

21 Y. L. Song, M. Shen, H. Peng, C. Y. Wang, S. F. Zhao, Y. Zuo and L. D. Xie, Solubility of Cr_2O_3 in Molten Fluorides with Different ZrF_4 Contents and Fluoroacidities, *J. Electrochem. Soc.*, 2020, **167**, 023501.

22 ORNL-3419, *Molten-salt Reactor Program: Semiannual Progress Report for Period Ending*, Oak Ridge National Laboratory, 1963.

23 ORNL-1771, *Aircraft Nuclear Propulsion Project: Quarterly Progress Report for Period Ending*, Oak Ridge National Laboratory, 1954.

24 H. Peng, M. Shen, C. Y. Wang, T. Su, Y. Zuo and L. D. Xie, Electrochemical investigation of the stable chromium species in molten FLINAK, *RSC Adv.*, 2015, **5**, 76689–76695.

25 H. Mediaas, J. Vinstad and T. Østvold, *Solubility of MgO in $MgCl_2$–NaCl–NaF Melts, Minerals*, Metals and Materials Society, Warrendale, PA (United States), 1996.

26 G. Kipouros, H. Mediaas, J. Vindstad, T. Oestvold and O. Tkatcheva, *Oxide Solubilities and Phase Relations in the System Mg–Nd–O–Cl*, Minerals, Metals and Materials Society, Warrendale, PA (United States), 1996.